J|A|C|S
ARTICLES
Published on Web 03/02/2004

The Bond-Forming Reactions of Atomic Dications with Neutral Molecules: Formation of $ArNH^+$ and ArN^+ from Collisions of Ar^{2+} with NH_3

Natalie Lambert, Dominic Kearney, Nikolas Kaltsoyannis,* and Stephen D. Price*

Contribution from the Department of Chemistry, University College London, 20 Gordon Street, London WC1H 0AJ, U.K.

Received September 29, 2003; E-mail: n.kaltsoyannis@ucl.ac.uk; s.d.price@ucl.ac.uk

Abstract: An experimental and computational study has been performed to investigate the bond-forming reactivity between Ar^{2+} and NH_3. Experimentally, we detect two previously unobserved bond-forming reactions between Ar^{2+} and NH_3 forming ArN^+ and $ArNH^+$. This is the first experimental observation of a triatomic product ion ($ArNH^+$) following a chemical reaction of a rare gas dication with a neutral. The intensity of $ArNH^+$ was found to decrease with increasing collision energy, with a corresponding increase in the intensity of ArN^+, indicating that ArN^+ is formed by the dissociation of $ArNH^+$. Key features on the potential energy surface for the reaction were calculated quantum chemically using CASSCF and MRCI methods. The calculated reaction mechanism, which takes place on a singlet surface, involves the initial formation of an Ar−N bond to give $Ar-NH_3^{2+}$. This complexation is followed by proton loss via a transition state, and then loss of the two remaining hydrogen atoms in two subsequent activationless steps to give the products $^3ArN^+ + H^+ + 2H$. This calculated pathway supports the sequential formation of ArN^+ from $ArNH^+$, as suggested by the experimental data. The calculations also indicate that no bond-forming pathway exists on the ground triplet surface for this system.

1. Introduction

The gas-phase reactions between dications and molecules are of importance in the context of "extreme" environments such as planetary atmospheres, the interstellar medium, and other natural and man-made plasmas.[1−3] However, until recently, studies of gas-phase ion−molecule reactivity have concentrated on monocation−molecule interactions. This focus is not surprising when one considers that, following an ionizing event, the majority of products are monocationic. This dominance of monocationic products is due to their stability, relatively long lifetimes, and the larger cross sections for single ionization[4−7] than for multiple ionization. However, in the last two decades, it has been shown that many molecular doubly charged ions (dications) possess one or more long-lived ($\tau \geq \mu$s) metastable electronic states.[8,9] In addition, the double ionization cross sections of many dication precursors have been shown to be largely underestimated in most early experiments due to the inefficient detection of the highly energetic products of double ionization.[5−7,10−13] In light of these discoveries, interest in dication−molecule reactivity has been growing steadily since the 1980s. These efforts have revealed a rich and varied dication−molecule chemical reactivity. For example, experimental studies have shown that, at both high (keV) and low (eV) collision energies, the major ionic products of dication−molecule reactions are often two singly charged species; that is, a single electron transfer occurs from the neutral species to the dication (eq 1):[8,9,14,15]

$$X^{2+} + Y_2 \rightarrow X^+ + Y_2^+ \qquad (1)$$

However, such electron-transfer reactions are not the only possible outcome of dication/neutral collisions. Bimolecular bond-forming reactions can also occur, in which chemical bonds are made, broken, and rearranged within the collision system. In 1989, it was shown that the molecular oxygen dication reacts with NO to yield NO_2^+ and O^+.[16] Stimulated by this study, Price and co-workers[17] investigated the bimolecular reactivity of 44 molecular dication/neutral collision systems. This survey revealed a large number of bond-forming reactions. Since this

(1) Prasad, S.; Furman, D. R. *J. Geophys. Res.* **1975**, *80*, 1360.
(2) Nicolaides, C. A. *Chem. Phys. Lett.* **1989**, *161*, 547.
(3) Witasse, O.; Dutuit, O.; Lilensten, J.; Thissen, R.; Zabka, J.; Alcaraz, C.; Blelly, P. L.; Bougher, S. W.; Engel, S.; Anderson, L. H.; Seiersen, K. *Geophys. Res. Lett.* **2002**, *29*, 1263.
(4) Ma, C.; Bruce, M. R.; Bonham, R. A. *Phys. Rev. A* **1991**, *44*, 2921.
(5) Bruce, M. R.; Bonham, R. A. *Int. J. Mass Spectrom.* **1993**, *123*, 97.
(6) Calandra, P.; O'Conner, C. S. S.; Price, S. D. *J. Chem. Phys.* **2000**, *112*, 10821.
(7) Harper, S.; Calandra, P.; Price, S. D. *Phys. Chem. Chem. Phys.* **2001**, *3*, 741.
(8) Price, S. D. *J. Chem. Soc., Faraday Trans.* **1997**, *93*, 2451.
(9) Herman, Z. *Int. Rev. Phys. Chem.* **1996**, *15*, 299.
(10) Bruce M. R.; Ma, C.; Bonham, R. A. *Chem. Phys. Lett.* **1992**, *190*, 285.
(11) Lindsay, B. G.; Mangan, M. A.; Straub, H. C.; Stebbings, R. F. *J. Chem. Phys.* **2000**, *112*, 9404.
(12) Straub, H. C.; Lindsay, B. G.; Smith, K. A.; Stebbings, R. F. *J. Chem. Phys.* **1998**, *108*, 109.
(13) Straub, H. C.; Lindsay, B. G.; Smith, K. A.; Stebbings, R. F. *J. Chem. Phys.* **1996**, *105*, 4015.
(14) Newson, K. A.; Price, S. D. *Chem. Phys. Lett.* **1997**, *269*, 93.
(15) Kearney, D. J. A.; Price, S. D. *Phys. Chem. Chem. Phys.* **2003**, *5*, 1575.
(16) Chatterjee, B. K.; Johnsen, R. *J. Chem. Phys.* **1989**, *91*, 1378.
(17) Price, S. D.; Manning, M.; Leone, S. R. *J. Am. Chem. Soc.* **1994**, *116*, 8673.

10.1021/ja038779a CCC: $27.50

initial work, a significant number of both experimental and theoretical investigations of the mechanisms, dynamics, and energetics of the bond-forming reactions of molecular dications with neutrals have been performed.[8,9,14,15,17−25]

Despite this focus on the chemical reactivity of molecular dications, the bond-forming reactivity of atomic dications with neutrals has received less attention, particularly at low collision energies. In 1986, bond-forming reactions were identified following collisions between atomic transition metal dications and alkanes.[18,26,27] Perhaps more surprisingly, a bond-forming reaction between Ar^{2+} and N_2 was recently observed by Tosi et al. (eq 2),[28] in which a doubly charged molecular product was detected for the first time:

$$Ar^{2+} + N_2 \rightarrow ArN^{2+} + N \qquad (2)$$

Following this study, Tosi et al. also reported the formation of ArC^{2+} from collisions of Ar^{2+} with CO and CO_2,[29] and Ascenzi et al. detected ArO^+ and ArO^{2+} products following collisions of Ar^{2+} with O_2.[30] Estimates of the integral cross sections for these reactive processes are of the order of 0.1 A^2 or smaller.[28,30]

In the current paper, we present the results of a series of experiments using time-of-flight mass spectrometry (TOFMS) to quantify the products following collisions between Ar^{2+} and NH_3. In these experiments, we detect both $ArNH^+$ and ArN^+, and we also find that the ratio of the experimental ion intensities of these two products, $I[ArN^+]/I[ArNH^+]$, increases with collision energy. This collision energy dependence is interpreted as resulting from an increasing propensity for $ArNH^+$ fragmentation with increasing available energy.

There currently exist only five published accounts of quantum chemical investigations of bond-forming dication−neutral reactions. The first of these, by Mrázek et al.,[22] presented the calculated ground-state stationary points on the potential energy surface of the reaction $CO_2^{2+} + H_2 \rightarrow HCO^+ + H^+ + O$. The geometric parameters of the stationary points along this potential energy surface were provided in a later study by Tafadar et al.[31] A recent study by Roithová et al.[32] characterized the stationary points on the potential energy surfaces leading to the formation of the bond-forming product ion $CHDCl^+$ from collisions of the $[CHCl]^{2+}$ dication with D_2. We have also recently completed an investigation of the potential energy surface for the bond-forming reaction between CF_2^{2+} and H_2O to give OCF^+, H^+, and HF.[33] All three of these reactions appear to proceed via similar mechanisms, in which a collision complex is formed between the dication and the neutral, followed by internal H atom rearrangement and finally fragmentation of the complex to products. Ascenzi et al. have also provided the energetics of the entrance and exit channels for the bond-forming reaction pathways that result from collisions of Ar^{2+} with O_2,[30] showing that the formation of the ArO^+ and ArO^{2+} product ions in their ground and some excited states is exothermic.

In this paper, to complement the experimental results, we present a quantum chemical investigation of the key features of the calculated potential energy surface (PES) for the bond-forming reaction $Ar^{2+} + NH_3 \rightarrow ArN^+ + H^+ + 2H$, which reveals a reaction pathway that is consistent with the experimental data. Significantly, we find that the bond-forming pathway lies on a singlet potential energy surface and is not accessible for Ar^{2+} in its ground (^3P) state.

2. Experimental Details

The apparatus used in these studies has been described in detail before,[8,14] and a diagram of the experimental apparatus is shown in Figure 1. Briefly, reactant dications are produced by electron ionization of a suitable precursor gas. In this case, Ar is introduced into the source region and is bombarded with 100 eV electrons to yield predominantly monocations and dications. The pressure of Ar as measured by an ion gauge is 5×10^{-6} mbar, low enough to ensure very few ion−neutral collisions. It is well established that electron ionization of the heavier rare gases results, at high electron energies (around 200 eV), in a beam comprised of an approximately statistical distribution of the ^3P, ^1D, and ^1S states from the ground (np^4) electronic configuration of the dication.[34] Thus, we would expect our Ar^{2+} ion beams to contain both singlet and triplet states arising from the $3p^4$ configuration. Indeed, the reactions of both singlet and triplet states in such beams have been observed.[35,36] The ions resulting from the electron impact are then extracted from the ionization region, collimated by various optics, and focused into a velocity filter. The dication of interest, in this case Ar^{2+}, is selected by a velocity filter, and the resulting dication beam is decelerated to the required collision energy. The dications then enter the source region of a TOFMS, which also serves as the ion−molecule collision region. The neutral collision gas, NH_3, is admitted into the interaction region as an effusive jet, at right angles to the incident dication beam. Both the product and the reactant ions are then extracted from the source region and identified and quantified by time-of-flight mass spectrometry. To achieve this, the voltage on the repeller plate in the source region is pulsed from 0 to +400 V. For each such pulse, a "start" signal is sent to the time to digital converter (TDC). The voltage pulse extracts both the unreacted dications and the product ions from the source region of the TOFMS, which is oriented orthogonally to both the incident dication beam and the jet of neutral species. These unreacted dications and product ions are then accelerated through a second acceleration region and into a field free drift zone. The ions are then detected by a pair of microchannel plates (MCP). When an ion reaches the MCP detector, the resulting signal is presented to a constant fraction discriminator (CFD) which generates a "stop" signal for the TDC. The difference between these start and stop signals is the time-of-flight for an ion. The flight time for each ion detected is added to a histogram, which makes up a complete mass spectrum. The intensity of an ion signal is given by the area of its peak in this mass spectrum, which corresponds to the number of ions detected with that particular range of flight times. The pressure of the neutral collision gas in the interaction region is carefully maintained throughout the

(18) Tonkyn, R.; Weisshaar, J. C. *J. Am. Chem. Soc.* **1986**, *108*, 7128.
(19) Armentrout, P. B. *ACS Symp. Ser.* **1992**, 502.
(20) Dolejšek, Z.; Fárník, M.; Herman, Z. *Chem. Phys. Lett.* **1995**, *235*, 99.
(21) Herman, Z.; Žabka, J.; Dolejšek, A.; Fárník, M. *Int. J. Mass Spectrom.* **1999**, *192*, 191.
(22) Mrázek, L.; Žabka, J.; Dolejšek, Z.; Hrušák, J.; Herman, Z. *J. Phys. Chem.* **2000**, *104*, 7294.
(23) Newson, K. A.; Price, S. D. *Chem. Phys. Lett.* **1998**, *294*, 223.
(24) Newson, K. A.; Tafadar, N.; Price, S. D. *J. Chem. Soc., Faraday Trans.* **1998**, *94*, 2735.
(25) Schröder, D.; Schwarz, H. *J. Phys. Chem. A* **1999**, *103*, 7385.
(26) Roth, L. M.; Freiser, B. S. *Mass Spectrom. Rev.* **1991**, *10*, 303.
(27) Chem, Q.; Auberry, K. J.; Freiser, B. S. *Int. J. Mass Spectrom.* **1998**, *175*, 1.
(28) Tosi, P.; Correale, R.; Lu, W.; Falcinelli, S.; Bassi, D. *Phys. Rev. Lett.* **1999**, *82*, 450.
(29) Tosi, P.; Lu, W.; Correale, R.; Bassi, D. *Chem. Phys. Lett.* **1999**, *310*, 180.
(30) Ascenzi, D.; Franceschi, P.; Tosi, P.; Bassi, D.; Kaczorowska, M.; Harvey, J. N. *J. Chem. Phys.* **2003**, *118*, 2159.
(31) Tafadar, N.; Kearney, D.; Price, S. D. *J. Chem. Phys.* **2001**, *115*, 8819.
(32) Roithová, J.; Hrušák, J.; Herman, Z. *J. Phys. Chem. A* **2003**, *107*, 7355.
(33) Lambert, N.; Kaltsoyannis, N.; Price, S. D. *J. Chem. Phys.* **2003**, *119*, 1421.
(34) Fukuroda, A.; Kobayashi, N.; Kaneko, Y. *J. Phys. B* **1989**, *22*, 3457.
(35) Smith, D.; Adams, N. G.; Alge, E.; Villinger, H.; Lindinger, W. *J. Phys. B* **1980**, *13*, 2787−2799.
(36) Hu, W. P.; Harper, S. M.; Price, S. D. *Meas. Sci. Technol.* **2002**, *13*, 1512.

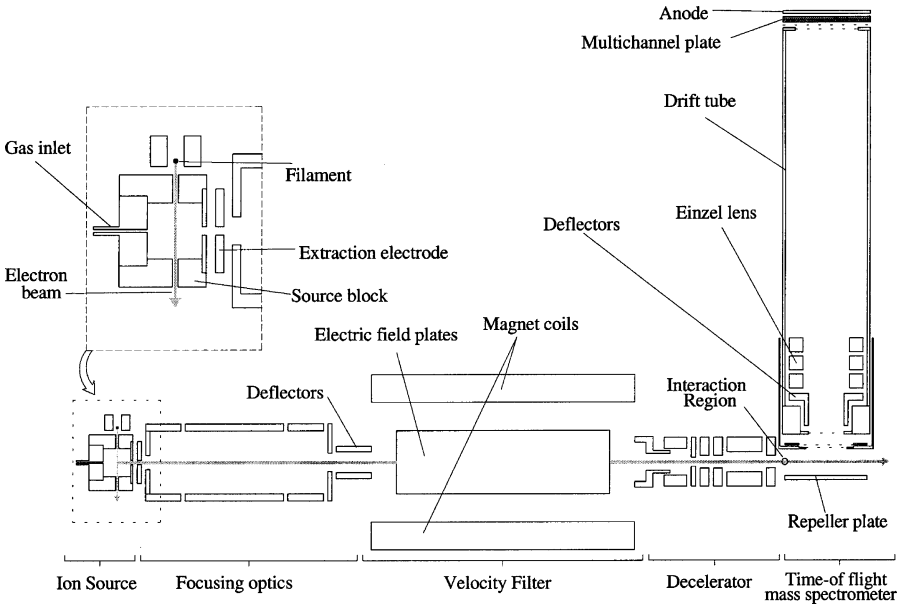

Figure 1. Diagram of the experimental apparatus used in this study. The TOFMS is positioned orthogonally to the incident dication beam.

experiment to ensure single collision conditions (a typical pressure is 4×10^{-6} Torr). Experiments were carried out at collision energies between 1 and 14 eV in the laboratory frame. The zero of energy is determined by both retarded field and time-of-flight analysis. Given the experimental conditions in this study, the energy uncertainty at each experimental collision energy is conservatively estimated to be ±0.2 eV in the LAB frame.

Our data processing procedures have been described before in the literature,[15] and only a brief overview follows. Each mass spectrum recorded following collisions between atomic dications and neutral molecules is corrected to allow for signals arising from stray ions within the chamber. These stray ions produce a small nonzero baseline in the mass spectrum. Mass spectra are also recorded in the absence of the neutral collision gas. Any relevant ion signals in such "collision gas free" spectra are appropriately normalized and then subtracted from the product ion signals recorded in the presence of collision gas. This correction removes any contribution to the final ion signals from collisions between the reactant dication and residual gas present within the chamber or from impurities present in the dication beam. This correction is very small, typically only a few percent of the total product ion signal. At least three sets of spectra were recorded at each collision energy. A single set of spectra comprises three spectra recorded with the collision gas on and two with the collision gas off.

3. Computational Details

The key features on the potential energy surface (PES) for the reaction $Ar^{2+} + NH_3 \rightarrow ArN^+ + H^+ + 2H$ were calculated. In certain regions of the PES, such as those associated with H atom loss from singlet structures such as $ArNH_3^{2+}$ and $ArNH_2^+$, we observed high (>2%) values of the T_1-diagnostic in trial CCSD(T)//B3LYP calculations. The T_1-diagnostic is a measure of the singles amplitudes in the CCSD(T) matrix and is typically used as a guide for the quality of the wave function. A T_1-diagnostic of greater than 2% is generally interpreted as an indication that the single-reference wave function is not accurately describing the system. We therefore employed multireference methods in all of the calculations reported here.

Geometry optimizations were performed using the complete-active-space multiconfigurational self-consistent field (CASSCF) method and the aug-cc-pvtz basis set. A full valence active space was used, where the N 1s and the Ar 1s, 2s, and 2p atomic orbitals were kept inactive but allowed to relax during the geometry optimizations. The resulting wave functions consisted of up to 32 000 configuration state functions (CSF). No symmetry constraints were imposed during the geometry optimizations. Vibrational frequency analyses were used to obtain zero-point energies and to characterize the transition states, and intrinsic reaction coordinate (IRC) calculations were performed on all transition states to verify that they are indeed on the same reaction path as their adjacent minima.

Single-point energy calculations were then performed on the CASSCF-optimized geometries using the multireference configuration interaction (MRCI) method with the same basis set. The same full valence active space as we employed for the geometry optimizations was used. To minimize computational costs, only those reference configurations with a weight greater than 0.01 were selected. For each calculation, the square of the normalization coefficient for the wave function made up from these selected configurations was always greater than 0.997. The CASSCF[37,38] and MRCI[39,40] calculations were carried out using MOLPRO v.2002.3.[41]

4. Results and Discussion

4.1. Experimental Results. Mass spectra were recorded following collisions between Ar^{2+} and NH_3 at center-of-mass frame collision energies of between 0.3 and 4.2 eV (1−14 eV in the laboratory frame). After the corrections described in section 2 have been applied, the spectra show the presence of H^+, N^+, NH^+, NH_2^+, NH_3^+, Ar^+, ArN^+, and $ArNH^+$. All of these ions except ArN^+ and $ArNH^+$ may be assigned as the products of dissociative and nondissociative electron-transfer reactions. The competition between dissociative and nondissociative electron transfer can be readily explained by the degree of internal excitation in the primary products (Ar^+ and NH_3^+) of the electron-transfer process. If stable states of NH_3^+ are populated, nondissociative electron transfer results. Conversely, if dissociative states are populated, the NH_3^+ ion fragments to yield a daughter ion. Electron-transfer reactions of atomic and

(37) Werner, H.-J.; Knowles, P. J. *J. Chem. Phys.* **1985**, *82*, 5053.
(38) Knowles, P. J.; Werner, H.-J. *Chem. Phys. Lett.* **1985**, *115*, 259.
(39) Werner, H.-J.; Knowles, P. J. *J. Chem. Phys.* **1988**, *89*, 5803.
(40) Knowles, P. J.; Werner, H.-J. *Chem. Phys. Lett.* **1988**, *145*, 514.
(41) MOLPRO is a package of ab initio programs written by H.-J. Werner and P. J. Knowles, with contributions from R. D. Amos, A. Bernhardsson, A. Berning, P. Celani, D. L. Cooper, M. J. O. Deegan, A. J. Dobbyn, F. Eckert, C. Hampel, G. Hetzer, T. Kornoa, R. Lindh, A. W. Lloyd, S. J. McNicholas, F. R. Manby, W. Meyer, M. E. Mura, A. Nicklass, P. Palmieri, R. Pitzer, G. Rauhut, M. Sch'utz, H. Stoll, A. J. Stone, R. Tarroni, and T. Thorsteinsson.

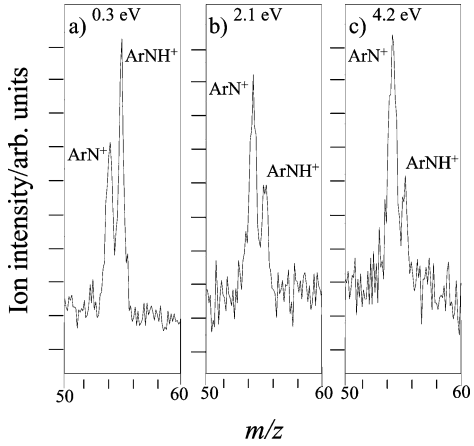

Figure 2. Mass spectra at (a) 0.3, (b) 2.1, and (c) 4.2 eV collision energy in the center-of-mass frame showing the signals corresponding to ArN^+ and $ArNH^+$ detected following collisions of Ar^{2+} with NH_3. The spectra clearly show that the ratio of ArN^+ to $ArNH^+$ increases with increasing collision energy. Processing the intensities of the ArN^+ and $ArNH^+$ ions in these spectra[15] indicates that, as the mass spectra show, the sum of the reactive cross sections for forming these product ions is constant, within experimental error, over this range of collision energies.

molecular dications, in this collision energy regime, have been shown to be well modeled by the Landau−Zener reaction window theory.[42−44] The details of the electron-transfer reactivity in this collision system will be discussed in a future publication and will not be considered any further in this Article.

The ions ArN^+ and $ArNH^+$, corresponding to $m/z = 54$ and 55, respectively, clearly come from bond-forming chemical reactions. Representative mass spectra, as a function of collision energy, are shown in Figure 2. As is often the case, the cross sections for forming these new adduct ions are small as compared with those of the electron-transfer reactions observed in the same collision system. For example, the total signal arising from ArN^+ and $ArNH^+$ is only approximately 5% of the signal arising from the electron-transfer product Ar^+.

As has been discussed before in the literature, we must always consider the possibility that mass discriminating effects operate in our TOFMS apparatus.[15] However, as shown below, we are confident that such effects do not significantly affect the relative detection efficiency of ArN^+ and $ArNH^+$ in the present experiments. Mass discrimination between different product ions can arise in our apparatus as a result of the differing kinetic energies that these ions can possess perpendicular to the axis of the TOFMS. A significant velocity component transverse to the axis of the TOFMS may result in ions striking the walls of the drift tube and not reaching the detector. Ions with different transverse kinetic energies will not travel the same transverse distance as they fly down the TOFMS. Thus, there is the possibility of varying fractions of the product ions being detected, a different detection efficiency for ions of different mass. To estimate any variations in detection efficiency for the product ions, we can calculate the length of the source region from which ions reach the detector, for a given transverse kinetic energy of the ion. To estimate the transverse kinetic energy of the product ions of dication reactions, we use the fact that the kinetic energy release for these reactions is dominated by electrostatic repulsion, giving an energy release of approximately

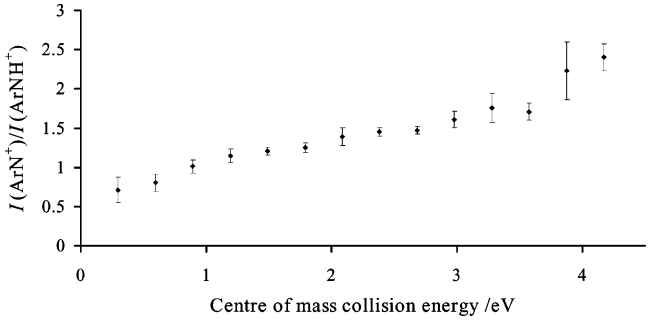

Figure 3. A plot of $I(ArN^+)/I(ArNH^+)$ versus collision energy. $I(ArN^+)/I(ArNH^+)$ clearly increases with collision energy.

7 eV, and these reactions are experimentally observed to involve forward scattering.[9,21,22,45] When we correct our mass spectral data in the above manner, to allow for any transverse ion losses, we produce relative ion intensities in good agreement with other measurements in the literature.[15] However, for the detection of ArN^+ and $ArNH^+$, because the ions have very similar masses, the relative discrimination between these ions is small. For example, given the mechanistic conclusions presented below, we consider the ArN^+ and $ArNH^+$ to be formed via a charge separating dissociation of $ArNH_3^{2+}$ to $ArNH_2^+ + H^+$, with the $ArNH_2^+$ subsequently dissociating sequentially to yield $ArNH^+$ and eventually ArN^+. For this mechanism, we calculate that our detection efficiencies as a function of center-of-mass kinetic energy are the same (within 3%) for ArN^+ and $ArNH^+$. Hence, we conclude that our relative detection efficiency of ArN^+ and $ArNH^+$ is the same within experimental error over the experimental range of collision energies we employ. Identical conclusions have been reached before for the relative detection efficiency in our apparatus of product ions with similar masses, resulting in experimental data which agree well with those in the literature.[14] Hence, we consider the ratio of intensities $I[ArN^+]/I[ArNH^+]$, which we derive from our mass spectra to be representative of the ratio of the cross sections of the reactive processes forming these ions.

Figure 3 shows the ratio of the bond-forming product ion intensities, $I[ArN^+]/I[ArNH^+]$, as a function of collision energy. The figure clearly shows that $I[ArN^+]/I[ArNH^+]$ increases with increasing collision energy. Figure 2 demonstrates that an increase in the ArN^+ ion yield is accompanied by a corresponding decrease in the $ArNH^+$ ion yield. This variation is consistent with ArN^+ being formed via the dissociation of $ArNH^+$.

4.2. Computational Results. Figure 4 shows the stationary points calculated along the PES of the reaction of Ar^{2+} with NH_3 to produce $ArNH^+$ and ArN^+. The mechanism first involves the formation of the Ar−N bond to give $ArNH_3^{2+}$, the global minimum for the pathway. This is followed by loss of a proton from the complex via transition state 1 with an activation energy of 5.74 eV to give $ArNH_2^+ + H^+$. An H atom then dissociates from $ArNH_2^+$ to leave $ArNH^+ + H$. The last remaining H atom can also dissociate from $ArNH^+$, leaving $^3ArN^+$ and an H atom in their ground states. The final products are hence $^3ArN^+ + H^+ + 2H$. For each stationary point, geometric parameters and symmetries are given in Table 1, and the total energies and zero-point energy corrections are given in Table 2.

(42) Rogers, S. A.; Price, S. D.; Leone, S. R. *J. Chem. Phys*. **1993**, *98*, 280.
(43) Zener, C. *Proc. R. Soc. London, Ser. A* **1932**, *137*, 696.
(44) Landau, L. *Phys. Z. Sowjetunion* **1932**, *2*, 26.
(45) Herman, Z.; Jonathan, P.; Brenton, A. G.; Beynon, J. H. *Chem. Phys. Lett.* *141*, 433.

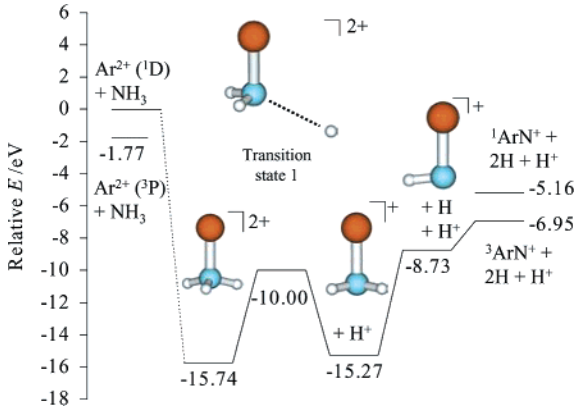

Figure 4. The calculated stationary points on the potential energy surface for the reaction $^1Ar^{2+} + NH_3 \rightarrow ArN^+ + H^+ + 2H$.

Table 1. Geometric Parameters of CASSCF-Optimized Structures on the Singlet Potential Energy Surface for $Ar^{2+} + NH_3 \rightarrow {}^3ArN^+ + H^+ + 2H$ (See Figures 4 and 6)[a]

structure	Ar–N	N–H	Ar–N–H	H–N–H
$^1NH_3$		1.022 [3]		105.1° [3]
$^1ArNH_3^{2+}$	1.817	1.056 [3]	105.0° [3]	113.6° [3]
transition state 1 (singlet)	1.863	1.042 [2], 2.811	98.61° [2], 118.9°	115.3° [2], 107.6°
transition state 2 (singlet)	1.825	1.056 [2], 2.522	99.87°, 126.1°	134.1°
$^1ArNH_2^+$	1.951	1.044 [2]	95.80° [2]	104.6°
$^2ArNH_2^{2+}$	1.737	1.065 [2]	114.1° [2]	132.0°
$^2ArNH^+$	1.911	1.059	96.05°	
$^3ArN^+$	1.886			
$^1ArN^+$	1.841			

[a] All bond distances are in angstroms (Å). The number of degenerate bond lengths and angles are given in square brackets. No symmetry constraints were imposed during the calculations.

Table 2. MRCI Total Energies and Zero-Point Energy Corrections for Optimized Structures on the Singlet Potential Energy Surface for $Ar^{2+} + NH_3 \rightarrow {}^3ArN^+ + H^+ + 2H$ (See Figures 4 and 6)

structure	total energy/ hartrees	zero-point energy correction/hartrees
NH_3	−56.46732203	0.03385888
$^1ArNH_3^{2+}$	−582.44642014	0.03827394
transition state 1 (singlet)	−582.22404000	0.02695533
transition state 2 (singlet)	−581.60535030	0.01298255
$^1ArNH_2^+$	−582.41605214	0.02516017
$^2ArNH_2^{2+}$	−581.72068632	0.02205933
$^2ArNH^+$	−581.66198209	0.01108234
$^3ArN^+$	−581.08684331	0.00122156
$^1ArN^+$	−581.02111624	0.00126389
$^3Ar^{2+}$	−525.46144255	
$^1Ar^{2+}$	−525.39628688	
H	−0.49982118	

The calculated mechanism shown in Figure 4 confirms that $ArNH^+$ and ArN^+ are formed from the same reactive channel, as indicated by the experimental results. It is interesting to note that the bond-forming dication complex $ArNH_3^{2+}$ is found to be stable with respect to dissociation to $Ar^+ + NH_3^+$ only when formed in the singlet state; attempts to converge a geometry optimization to a stable triplet structure were unsuccessful. Such an effect is not surprising when one considers that the lowest energy electronic configuration of the triplet $ArNH_3^{2+}$ complex involves the promotion of an electron from a bonding to an antibonding orbital, lowering the Ar−N bond order and increasing the total energy of the complex. Therefore, it appears that only singlet states of Ar^{2+}, not the ground triplet state, contribute to bond-forming reactivity in this system.

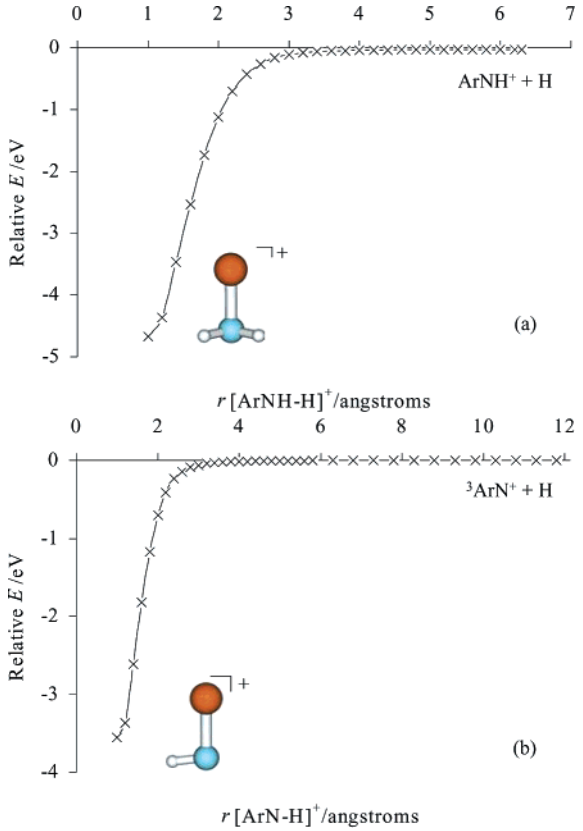

Figure 5. The results of a series of restricted geometry optimizations tracing the final two stages of the reaction mechanism shown in Figure 4: (a) the dissociation of $ArNH_2^+$ to $ArNH^+ + H$; (b) the dissociation of $ArNH^+$ to $^3ArN^+ + H$. In both cases, all geometric parameters were allowed to optimize at each point except for one N−H bond distance *r*, which is plotted on the *x*-axis. Energies are given relative to the sum of the energies of the fully optimized ground-state geometries of the products.

As can be seen in Figure 4, the loss of an H atom both from $ArNH_2^+$ and from $ArNH^+$ does not proceed via a transition state. To verify that the last two steps of the reaction mechanism are indeed activationless, a series of restricted geometry optimizations were performed to map the potential energy surface for removal of an H atom from $ArNH_2^+$ and from $ArNH^+$. In both cases, all geometric parameters were optimized except for the N−H bond distance corresponding to the reaction coordinate *r*, which was held fixed over a range of values between 1.0 and 6.3 Å for the dissociation of $ArNH_2^+$ and between 1.0 and 11.8 Å for the dissociation of $ArNH^+$. Due to a nearby curve crossing with the $ArNH + H^+$ pathway, restricted geometry optimizations for the dissociation of $ArNH_2^+$ were not continued past $r =$ 6.3 Å. These calculations were performed using the CASSCF method and aug-cc-pvtz basis set as described above. It should be noted that to successfully plot the surface for the dissociation of $ArNH_2^+$ to $ArNH^+ + H$, a slightly larger active space than that used for the $ArNH_2^+$ stationary point was needed. Although this larger active space may result in a lowering of the relative energies, the shape of the surface is not expected to change.

The results of the restricted geometry optimizations are shown in Figure 5. All energies are given relative to the sum of the energies of the products, calculated individually. These plots clearly show the lack of an activation barrier for the loss of an H atom from either $ArNH_2^+$ or $ArNH^+$. Such a result is not surprising, as the reverse processes correspond to attractive cation−neutral associations. Figure 5b also shows that the energy of the dissociation limit corresponds to that of the

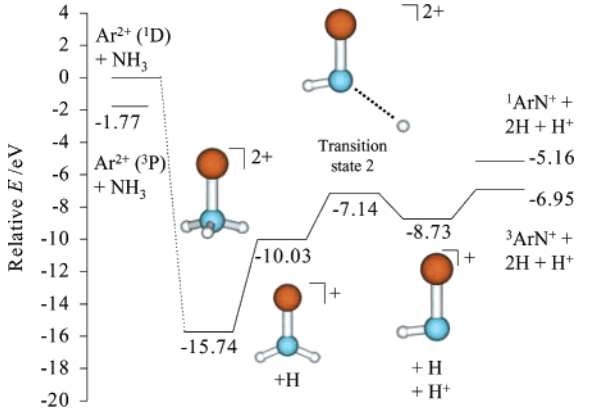

Figure 6. A schematic representation of the stationary points on the potential energy surface of an alternate pathway for the reaction $^1Ar^{2+} + NH_3 \rightarrow {}^3ArN^+ + H^+ + 2H$, in which the adduct dication decomposes via neutral loss, not charge transfer (see Figure 4).

$^3ArN^+ + H$ product asymptote, confirming that ArN^+ is formed in its ground triplet state.

As can be seen in Figure 4, breaking an N−H bond in the $ArNH_2^+$ ion requires an excitation of 6.54 eV, and breaking the N−H bond in the $ArNH^+$ complex requires an additional 1.78 eV. The reactants lie at an energy of 15.27 eV above the $ArNH_2^+ + H^+$ asymptote; therefore, every reactive event in principle begins with enough energy to reach completion and form ArN^+. However, such an analysis neglects the energy removed from the system, in the form of kinetic energy, during the charge separating dissociation of $ArNH_3^{2+}$ to form $ArNH_2^+$ and H^+. The measured kinetic energy release distributions for such processes are typically centered around 6−8 eV, with a width of several eV.[20−22] The loss of such large amounts of energy significantly reduces the internal energy content of the $ArNH_2^+$ ion. Specifically, for collisions at a center-of-mass energy of 0 eV, the charge-separating dissociation will reduce the internal energy contents of the $ArNH_2^+$ ions to a range of values from about −6 to −8 eV in Figure 4. Only those $ArNH_2^+$ ions that are formed with an internal energy of −6.95 eV or greater will proceed to the product asymptote $^3ArN^+ + H^+ + 2H$, while those $ArNH_2^+$ ions formed with less than −6.95 eV will only go as far as the $ArNH^+ + H^+ + H$ asymptote. With increasing collision energy, the residual internal energy of $ArNH_2^+$ will be higher, increasing the probability of complete dissociation to ArN^+. Thus, increasing the collision energy increases the yield of ArN^+ and correspondingly decreases the yield of $ArNH^+$, reproducing the behavior that we observe experimentally. Such sequential dissociations have been observed before for similar endothermic fragmentation steps in the bond-forming reactions between rare gas ions and molecules.[46−48]

It is also of interest to consider an alternative pathway to the formation of ArN^+ and $ArNH^+$ that involves neutral loss in the dissociation of $ArNH_3^{2+}$ rather than charge separation. The stationary points along this alternative pathway were calculated as described above, and the results are shown in Figure 6. The geometric parameters of $ArNH_2^{2+}$ and transition state 2 are given in Table 1. As can be seen in Figure 6, the neutral loss pathway is also consistent with the observed experimental collision energy dependencies of the formation of the $ArNH^+$ and ArN^+ ions. Assuming again 0 eV collision energy, the reactants will always have sufficient energy to form $ArNH^+$, because the amount of internal energy of the $ArNH_2^{2+}$ ion lost to the H atom in the neutral loss step should be small, less than 1 eV. However, the kinetic energy release of the charge separation of $ArNH_2^{2+}$ to $ArNH^+$ and H^+ will reduce the internal energy of $ArNH^+$ to approximately −6 to −8 eV (in Figure 6). As described above, in this situation again the probability of the $ArNH^+$ ion having enough internal energy to fragment to ArN^+ and H will increase with increasing collision energy. This would also result in the experimentally observed increase in the ArN^+ ion yield with a corresponding decrease in the $ArNH^+$ ion yield with increasing collision energy. In trying to decide which pathway is operating to form $ArNH^+$, we expect the pathway in which charge separation occurs first to be kinetically favored, as its rate-limiting transition state lies 2.86 eV lower in energy than that of the neutral loss pathway. In addition, we would expect a small dication such as $ArNH_3^{2+}$ to favor decay via initial charge separation to achieve the 5.24 eV stabilization of the $ArNH_2^+ + H^+$ state relative to the $ArNH_2^{2+} + H$ state. Indeed, the vast majority of dications derived from small molecules predominantly decay via charge separation rather than neutral loss.[21,22,49,50] Pathways such as the one shown in Figure 6, in which neutral loss occurs in the first step, may be of importance in larger systems where there is greater stabilization of the dipositive charge.

5. Conclusions

Crossed-beam collision experiments were performed between Ar^{2+} and NH_3. A previously unobserved bond-forming reaction channel, which leads to the formation of the molecular ions $ArNH^+$ and ArN^+, was detected. We believe this to be the first report of the formation of a triatomic molecular ion following a bond-forming reaction between a rare gas dication and a neutral. The product ion intensity $I[ArNH^+]$ was found to decrease with increasing collision energy, with a corresponding increase in the $I[ArN^+]$ product ion intensity, indicating that ArN^+ is formed by the dissociation of $ArNH^+$. The important features of the potential energy surface of the reaction were calculated quantum chemically and were found to be in agreement with the sequential mechanism suggested by the experimental results. These calculations reveal a reaction mechanism in which an $ArNH_3^{2+}$ complex is formed, and then loses a proton followed by two H atoms in three endothermic steps. An alternative mechanism in which the proton loss occurs following an initial H atom loss was also determined. It is expected that the pathway in which charge separation occurs first will be favored, because 2.86 eV less energy is required to overcome the rate-limiting transition state relative to H atom loss.

Acknowledgment. The authors are grateful for financial support from the Leverhulme Trust, to the European Union Network RTN1-2000-00027 "Generation, Stability, and Reaction Dynamics of Multiply Charged Ions" (MCInet) for support of N.L., and to the EPSRC for support of D.K. and for computing resources under grant GR/S06233/01. Thanks are also given to Jeremy Harvey and Detlef Schröder for valuable comments and suggestions.

JA038779A

(46) Ervin, K. M.; Armentrout, P. B. *J. Chem. Phys.* **1986**, *85*, 6380.
(47) Ervin, K. M.; Armentrout, P. B. *J. Chem. Phys.* **1987**, *86*, 6240.
(48) Ervin, K. M.; Armentrout, P. B. *J. Chem. Phys.* **1989**, *90*, 118.
(49) Larsson, M. *Comments At. Mol. Phys.* **1993**, *29*, 39.
(50) Curtis, D. M.; Eland, J. H. D. *Int. J. Mass Spectrom. Ion Processes* **1985**, *63*, 241.